Transient contact behavior of aqueous polymer solution droplets with transparent hot solid

AUTHOR(S):

Fujimoto, Hitoshi; Sakane, Shogo; Hama, Takayuki; Takuda, Hirohiko

CITATION:

Fujimoto, Hitoshi ...[et al]. Transient contact behavior of aqueous polymer solution droplets with transparent hot solid. Experimental Thermal and Fluid Science 2018, 96: 1-10

ISSUE DATE:

2018-09

URL:

http://hdl.handle.net/2433/237634

Transient contact behavior of aqueous polymer solution droplets with transparent hot solid

Hitoshi Fujimoto, Shogo Sakane, Takayuki Hama, and Hirohiko Takuda

Department of Energy Science and Technology, Graduate School of Energy Science, Kyoto University, Yoshida-honmachi, Sakyo-ku, Kyoto 606-8501, Japan

Abstract

In the metal forming industry, quench hardening is commonly used to strengthen steel products by rapidly cooling hot materials. One of the typical coolants used in the quench hardening process is an aqueous polymer solution. During the hardening process, several phenomena occur simultaneously, namely, coolant boiling, separation of the polymer from the aqueous solution, and formation of a polymer-enriched layer on the solid surface. The hydrodynamics and heat transfer characteristics of the coolant during the cooling process are complex in nature and remain unclear. The main objective of this study is to develop an experimental understanding of the collision and contact behavior of aqueous polymer solution droplets with a hot substrate. This research will serve as a fundamental reference work for the process of quench hardening using spray cooling. To fulfill this objective, a three-directional flash photography technique was developed. A transparent sapphire prism was used to observe the transient contact behavior of droplets with a hot solid, whose temperature was varied from 300 to 600 °C. A solution of 10 wt% polyoxyethylene-polyoxypropylene glycol with an average

molecular weight of approximately 20,000 was used as the test liquid. At a substrate temperature of 300 °C, jellylike polymer residue remained on the substrate. At 400 and 500 °C, a wet area appeared temporarily on the solid substrate soon after the droplet collision, but this area eventually disappeared because of the thermal decomposition of the polymer. At 600 °C, no wet area was seen. The lifetime of the temporary wet area decreased with an increase in the temperature of the solid but was almost independent of the impact inertia of droplets. In addition, in the case of the polymer solution droplet, the upper limit of the surface temperature for forming the wet area was around 580 °C, which was considerably higher than that in the case of a water droplet.

Keywords:

Flow visualization; polymer thermal decomposition; droplet dynamics

Nomenclature

c_p	specific heat, J/(kg K)
d	preimpact diameter of droplets, m
t	elapsed time after a droplet touches the solid surface, s
T_w	temperature of the solid substrate, °C
T_i	interfacial temperature at the moment of droplet impact, °C
v	impact velocity of the droplet, m/s
We	Weber number, -

Greek symbols

λ	thermal conductivity, W/(m K)
ρ	material density, kg/m^3
σ	surface tension, N/m

1. Introduction

Aqueous polymer solutions are widely utilized as a cooling medium in quench hardening processes to strengthen hot carbon steels [1–6]. Hot materials are rapidly cooled from approximately 750–900 °C to a certain specific temperature to induce martensitic transformation, and then, a moderate cooling rate is imposed on the materials to prevent unwanted quench-crack initiations or distortion of products. During the cooling process, the polymer separates from the aqueous solution and adheres to the material surface, resulting in the formation of a polymer-enriched layer [2], which is a characteristic feature of this coolant and inhibits rapid heat reduction from the solid substrate.

Several previous works [2–6] have focused on the cooling process in industrial heat-treatment applications using aqueous polymer solutions. The main interests of these studies were the measurement of the temperature histories of materials and the determination of the heat transfer coefficient. Various parameters were found to influence the heat transfer characteristics, including the polymer component, its concentration, and the cooling conditions. However, less attention has been paid to understanding the underlying physical mechanism. In general, actual cooling operation conditions are determined empirically without an understanding of the underlying physical mechanism. Indeed, to find better cooling operation conditions, it would be useful to have a fundamental understanding of the hydrodynamics and boiling phenomena of polymer quenchants, and the formation process of the polymer-enriched layer. The present study was not aimed at obtaining practical data for an actual cooling system design, but rather at an exploration of the fundamental physics of the phenomena through simple laboratory-scale experiments.

Spray cooling methods are commonly employed in induction hardening applications [5,6], in which steel products are heated by induction heating, followed by immediate quenching. The collision of individual liquid droplets with a solid is a basic process of

spray cooling applications [7,8]. Several excellent review papers concerning the collision of individual liquid droplets with a solid have been published [9-15]. In most previous works, a single-component liquid such as water or fuel was used. However, the deformation behavior of aqueous solution droplets with polymer additives has been less studied. Rozhkov et al. [16] studied the collision behavior of aqueous polymer solutions with small nonheated targets made of stainless steel by employing a high-speed photography technique. The test liquids were aqueous water solutions of polyethylene oxide at concentrations of 10, 100, and 1000 wt ppm. The droplet impacted the target, and a liquid lamella was formed. Polymeric additives were shown to prevent the rupture of the liquid lamella. Bertola [17] studied a droplet impacting a hot solid heated at 120–180 °C. The test liquids were water and a water solution with 0.02 wt% polyethylene oxide additives. The Weber number, which ranged from 20 to 220, is the ratio of the impact inertia to the surface tension force and is defined as

$$We = \frac{\rho v^2 d}{\sigma} \qquad (1)$$

where ρ, v, d, and σ represent the liquid density, impact velocity, droplet diameter, and surface tension coefficient of droplets, respectively. They reported the additive inhibited droplet splashing, secondary droplet ejection, and mist formation.

Bertola and Sefiane [18] studied the effects of minute amounts of polyethylene oxide in water on the occurrence of secondary atomization when a liquid drop impacted a heated surface at 150–350 °C. The additive was found to oppose the scattering of secondary droplets from the free surface of the liquid. Zang et al. [19] studied the impact dynamics of droplets on a superhydrophobic surface with a dendritic structure by using a high-speed camera. The test liquid contained silica nanoparticles and/or polyethylene oxide additives. They showed that both the particles and polymer additives constrain the instability behavior of the liquid.

The abovementioned works reported useful data from a scientific perspective, but the

experimental conditions used in these studies, including the polymer type, its concentration, and the temperature range of the solid substrate, were different from those in actual hardening processes of steel products. Therefore, we studied the hydrodynamic behavior of droplets of an aqueous polymer solution impinging on a hot sapphire substrate by employing a flash photography technique [20]. An aqueous solution of 10 wt% polyoxyethylene-polyoxypropylene glycol with an average molecular weight of approximately 20,000 was used as the test liquid. When the Weber number was small and the substrate temperature was 500 °C, the droplet impacted the solid, deformed into a disc, and recoiled and rebounded off the solid. Some empirical formulae for predicting the spreading diameter of droplets and the resident time were built as functions of the Weber number. More interestingly, a polymer-enriched layer was found to form temporarily on the hot substrate and eventually disappear because of the thermal decomposition of the polymer. This finding indicates that a polymer-enriched layer might be present even at a substrate temperature that is higher than the temperatures at which the test polymer is thermally decomposed. This is also interesting from an industrial perspective, because the polymer-enriched layer influences the transient temperature profile of materials during spray cooling. However, the process by which the polymer layer forms and disappears remains unclear, because the flow visualization technique used in the above study was inappropriate for observing the phenomenon.

To address this problem, the present study was planned as a part of a series of studies. The main objective of the present study was to understand the transient liquid–solid interfacial phenomena, which involve the boiling of water, the separation of the polymer from the aqueous solution, and the formation of a polymer-enriched layer on the solid surface. A new flash photography technique was developed to investigate the collision and contact behavior of droplets with a hot substrate simultaneously by expanding the flow visualization technique used in our previous studies [21]. A transparent rectangular prism made of sapphire was employed as the test substrate to observe the physics of the

phenomena directly at the liquid–substrate interface during droplet impact. We used sapphire because its thermal conductivity and thermal diffusivity are comparable to those of some steel alloys like stainless steel.

The test polymer solution was the same as that used in our previous study [20]. Water was also used as a test liquid for reference. The effects of varying the substrate temperature and the Weber number on the contact behavior of the aqueous polymer solution droplets with the solid substrate were investigated. We found that at 300 °C, some polymer residue remained on the substrate. At 400 and 500 °C, a polymer-enriched layer temporarily appeared on the solid substrate and then disappeared because of the thermal decomposition of the polymer. At 600 °C, no wet area was seen. The lifetime of the temporary polymer-enriched layer depended on the substrate temperature but was almost independent of the Weber number. The physics of these phenomena will be discussed in detail, from both scientific and industrial perspectives.

2. Experiments

2.1 Test polymer and test solution

In the present study, polyoxyethylene-polyoxypropylene glycol (chemical formula: $HO–(C_2H_4O)_a–(C_3H_6O)_b–(C_2H_4O)_c–H$) was used as the test polymer. The measured molecular weight of the test polymer was approximately 20,000, and the measured ratio of $(a+c)$:b was 75:25. Figure 1 presents the thermogravimetric curve showing the relationship between the temperature of the test polymer and its weight when the polymer with an initial weight of 100 g was heated from 20 to 700 °C at a heating rate of 5 °C/min. The weight of the test polymer remained almost unchanged when the temperature was below 300 °C. It sharply decreased in the temperature range between approximately 300 and 400 °C because the test polymer was thermally decomposed into small-molecule gasses. Most of the test polymer vanished at temperatures higher than

400 °C.

The test solution was made by diluting the test polymer using distilled water to 10 wt%. The measured physical properties of the test solution are listed in Table 1. The properties of water at 40 °C are also shown for reference. The test solution is colorless and transparent at room temperature. When the test solution is heated above a cloud point of 75 °C [22], the solubility of the polymer drastically decreases, and the separation of the polymer and water occurs.

2.2 Experimental setup

Figure 2 shows a schematic diagram of the experimental apparatus used to observe the impact phenomena of droplets on the heated surface. The setup was composed of three units: the droplet generator, test substrate mounted on the heater unit, and observation equipment for flash photography. The droplet generator was similar to that used in our previous study [20], except that a nozzle cooling unit was not included because of the restriction in setup space. In the present experiments, the preimpact diameters, d, of the aqueous polymer droplets were approximately 2.2 mm. The impact velocities, v, of the droplets on the substrate were approximately 0.9, 1.1, and 1.6 m/s, which were achieved by adjusting the nozzle-to-substrate distance. Distilled water droplets with diameters of approximately 2.4 mm were also used for reference.

The test substrate was a rectangular optical prism made of sapphire with a horizontal area of 20 × 20 mm; the droplets were made to impinge on the substrate. As the test prism was originally made for use in optical devices, it had a very smooth surface; the prism flatness, defined as the distance between the peak and valley of the prism, was within 320 nm. The rectangular prism was mounted on a stainless-steel heating unit equipped with three cartridge heaters. Slight movement of the test prism was allowed during experiments to avoid unwanted crack initiation of the test prism due to the difference in the thermal expansion rates of sapphire and stainless steel.

The substrate surface temperature was maintained at a preset value (300–600 °C) using a temperature controller and a K-type thermocouple. The accuracy of the temperature measurement was within 2.5 °C. An infrared camera was also used to monitor the surface temperature through a thin coat of black-body paint (emissivity: 0.94) applied to a part of the substrate surface. The droplets were always made to impinge on the uncoated part of the dry, cleaned substrate surface.

2.3 Photography technique

A three-directional photography technique was newly developed in the present study by expanding the flow visualization technique used in our previous studies [20,21]. The setup was composed of an optical sensor, a delay timer, a flash controller, four flash lights A_1, A_2, B, and C, and three digital cameras A, B, and C, as shown in Figure 2. The spatial resolution of cameras A and C was 5184 × 3456 pixels, and that of camera B was 3888 × 2592 pixels. Camera A, the test prism, and a pair of flashlights (A_1 and A_2) were aligned horizontally. The optical sensor captured the falling droplets and produced trigger signals for flash photography. When the droplets entered the observation area near the solid substrate, the two flashlights were activated consecutively at certain time intervals; side-view, doubly exposed, backlit images of the droplets were captured (Figure 3(a)). Camera B and flashlight B were arranged to capture top-view images of the droplets (Figure 3(b)). These images allow us to understand the three-dimensional motion of the droplets and the boiling phenomena inside the droplets. Descriptions of these two photography techniques can be obtained from our previous paper [21].

The images of the liquid–solid interface were captured from the direction obliquely behind the optical prism using camera C and flashlight C, as shown in Figure 4. Observation light from flashlight C entered an optical prism through a cylinder-shaped hole with a diameter of approximately 6.2 mm in the heater unit. The incident angle of the light to the solid surface on which the droplets impinged was 45°. The refractive

indices of air (vapor), water, the test solution, and sapphire were 1.0, 1.33, 1.35, and 1.75, respectively. Total reflection occurred at the air–sapphire interface according to Snell's law, whereas some light passed through the water–sapphire interface. The light exited the heater unit through a hole with a diameter of approximately 6.2 mm, was reflected by a mirror, and reached Camera C. Consequently, the interface images could be captured; the images indicated that the air (or vapor)–sapphire interface was bright, and the water (or test solution)–sapphire interface was relatively dark, as shown in Figure 3(c) [23, 24]. In addition, a circular wet area was exposed to form a horizontally long oval shape in the images because of the incident angle of the observation light to the interface (= 45°).

The time evolutions of the droplet shape and the contact behavior were followed by capturing many instantaneous images with various flash timings under the same impact conditions, assuming the repeatability of liquid motion. In each run, flashlight A_1 was activated before droplet impact to ensure that the preimpact diameter of the droplets was obtained. Then, flashlights A_2, B, and C were activated simultaneously with a preset delay. The three cameras were adjusted to capture images exclusively through flash photography. Thus, a set of three types of images was captured during each impact test, as shown in Figure 3. Note that more than 200 sets of images were taken for each experimental condition.

3. Results and discussion

3.1 Effect of varying substrate temperature on collision and contact behavior of droplets with sapphire substrate

The collision and contact behaviors of droplets with a hot substrate obtained by the developed flash photography technique are described in the present subsection. The experiments were performed by varying the temperature of the solid substrate, T_w, from 300 to 600 °C. Table 2 lists the experimental conditions under which the images shown

in different figures are obtained.

Figure 5 presents the time series of images showing the deformation behavior of aqueous polymer droplets impinging on the sapphire surface heated at T_w = 300 °C for (v, d) = (a) (1.6 m/s, 2.2 mm) (We = 106). The elapsed time (t) after droplet impact on a solid substrate is shown in each image. Top-view images of droplets, side-view images of droplets, and interface-view images are presented as the upper, middle, and bottom columns, respectively. Each set of three images was taken simultaneously by activating the three flash lights at the same time. In the side-view images, “red” droplets are always present above the impact point of the droplet on the solid. These red spots represent the images exposed at the first flash before droplet impact, as described previously. The horizontal scale is the same for all the images.

The polymer solution droplet touched the substrate at t = 0 s and deformed into a thin circular disc (0.1–2.0 ms). Boiling vapor bubbles were observed at the liquid–solid interface in the top-view images (0.1 and 0.4 ms). Some dark areas associated with the direct contact at the liquid–solid substrate spread with time in the interface view. The liquid–solid direct contact was larger than that for the water droplets, as shown in Figure 3. Then, small droplets were separated from the liquid body at 2.0 and 4.5 ms. In the time range of t = 7.2–38.5 ms, the apparent liquid–solid contact area was small in the side view, but the actual liquid–solid contact area in the interface view was larger and almost unchanged. Eventually, a jellylike polymer-enriched layer and/or some char always remained on the solid substrate, although they are not shown in the figures.

Figure 6(a) and (b) shows the images of the polymer solution droplets at T_w = 400 °C for (v, d) = (a) (1.5 m/s, 2.2 mm) (We = 103) and (b) (0.89 m/s, 2.2 mm) (We = 32), respectively. In this subsection, only the results for (a) (We = 103) are focused upon to investigate the effect of varying the temperature of the solid substrate on the droplet dynamics. The results for (b) (We = 32) will be discussed in subsection 3.2. In the interface view for (a), some dark areas appeared immediately after the droplet collision (t = 0.2 and 0.3 ms). Boiling bubbles were formed inside the liquid in the top view. In

the side view, many secondary droplets were formed because of bursting boiling bubbles at the liquid–air interface at t = 0.7 ms. From t = 1.4 to 2.7 ms, a bulge that was vertically elongated in the upward direction was observed in the center region of the droplet [20]. Small droplets were separated from the rim of the deforming liquid and flew radially outward. The droplets split into pieces at 4.5–6.9 ms, and most of the liquid moved away from the solid surface. At 42.0 and 98.0 ms, some mist was seen around the deforming liquid. The components of the mist were probably condensed vapor, the separated polymer, and/or thermally decomposed products of the polymer [20].

With regard to the interface view, the dark area increased in size with time at early times. After t = 5.7 ms, the dark area became small in size and light in gray-scale density. Some portion of the dark area was present even at 98 ms. Unlike the previous results for 300 °C, the dark area completely vanished at $t \approx$ 158 ms.

The experiments using water droplets were performed under similar Weber number conditions for reference. Figure 6(c) shows the images of the water droplets at T_w = 400 °C for (v, d) = (1.7 m/s, 2.4 mm) (We = 106). In the top view, the liquid–solid contact area appeared to be hazy immediately after droplet impact. At 3.1 and 3.9 ms, numerous secondary droplets were observed. Then, the droplet shuttered. In the interface view, only a few dark areas were present and only at 2.1 ms, indicating that the direct contact of the water (liquid)–substrate rarely occurred.

The critical boundary at which this direct contact does occur during droplet impact can be roughly explained in terms of the superheat limit of water and the temperature at the liquid–solid interface [21]. When a water droplet impacts a hot substrate, the liquid in the vicinity of the solid surface is heated abruptly. If the interfacial temperature is higher than the superheat limit of water (approximately 300 °C at 1 atmosphere pressure), explosive boiling occurs followed by the rapid formation of a vapor film between the liquid and the solid surface [25-34]. Because it is difficult to accurately measure the liquid–solid interfacial temperature experimentally, it is often estimated by

using the one-dimensional transient heat conduction theory for interfacial contact between two semi-infinite solids at different temperatures [35–41]. The interfacial temperature, T_i, is given by [42]

$$T_i = \frac{T_1\sqrt{\rho_1 c_{p1}\lambda_1} + T_2\sqrt{\rho_2 c_{p2}\lambda_2}}{\sqrt{\rho_1 c_{p1}\lambda_1} + \sqrt{\rho_2 c_{p2}\lambda_2}} \quad (2)$$

where T, ρ, c_p, and λ are the temperature, density, specific heat, and thermal conductivity, respectively, and subscripts 1 and 2 denote the two materials. The thermo-physical properties of water and sapphire are listed in Table 3. In the case of Figure 6(c), the evaluated interfacial temperature was 342 °C, which was higher than the superheat limit of water at atmospheric pressure. The experimental results were consistent with the results obtained using the above equation.

Nevertheless, Eq. (2) is probably inapplicable for estimating the interfacial temperature for polymer solution droplets, because the liquid is inhomogeneous above the cloud point. That is, the polymer separates. However, the results in Figure 6(c) suggest that the dark (wet) areas in Figure 6(a) formed because of the presence of the polymer. Because the local concentration of the test polymer was considered to be high in the dark (wet) areas, we refer to these areas as polymer-enriched in the present paper.

Incidentally, the temperature of the solid was considered to decrease sharply immediately after the droplet collisions and then recover to the initial temperature because of the heat conduction inside the solid substrate. Thus, Eq. (2) is valid in the very short period after the droplet collision. In addition, the dark areas in Figure 6(a) existed for a considerably longer time than the time scale of droplet hydrodynamics. The interfacial temperature at the polymer-enriched layer might be close to the initial temperature of the solid at later times, although we did not measure this. Judging from the thermogravimetric curve of the test polymer (Figure 1), the disappearance of the dark wet areas occurred because of the thermal decomposition of the test polymer.

Figure 7(a) and (b) shows the images of the polymer solution droplets at T_w = 500 °C for (v, d) = (a) (1.5 m/s, 2.2 mm) and (b) (0.88 m/s, 2.2 mm), respectively. The results

for (a) were focused upon in this subsection. In the top view for (a), the droplet impacted the solid surface, spread, deformed into a thin disc, and split into pieces. In the side view, secondary droplets were seen at 0.6 and 1.0 ms in the region of the advancing rim of the liquid. The main body of the liquid was distorted at 2.1 and 3.6 ms. At 14.0 and 20.2 ms, most of the small liquid masses moved away from the solid substrate. In addition, some mist was seen.

Some dark areas were seen in the interface view. The areas became darker with time for $t \leq 2.1$ ms and then became light. In addition, the intensity of lightness in the dark areas was higher than that for $T_w = 400$ °C, as shown in Figure 6(a). The dark areas disappeared as t reached 20.2 ms. The lifetime (disappearance time) of the dark areas was apparently shorter than that for $T_w = 400$ °C.

We attempted to perform experiments using water droplets for We ≈ 100 and T_w = 500 °C for reference, but they were unsuccessful. Immediately after water droplet impact, crack initiation due to abrupt thermal stress appeared on the solid substrate. The experiments for the water droplets could be performed without any occurrence of cracks for smaller values of impact inertia (We ≤ 80). As expected, dark areas associated with water–solid direct contact were not seen in the interface view at low We values. The results suggested that the dark areas in Figure 7(a) were formed because of the presence of the test polymer.

Incidentally, the interfacial temperature estimated by Eq. (2) was 424 °C at the water–sapphire interface for $T_w = 500$ °C. This value was higher than the temperature range for thermal decomposition, as shown in Figure 1. Although the actual interfacial temperature was not measured in the present study, a temporary polymer-enriched layer formed under such high-temperature conditions of the solid. Further, considering that crack initiation occurred for water droplets for We ≈ 100 and did not occur for polymer solution droplets, the polymer was inferred to have buffered the local thermal stress on the sapphire surface.

We also performed experiments at a low polymer concentration of the solution (= 5

wt%) at T_w = 500 °C. Figure 7(c) shows the images for (v, d) = (1.6 m/s, 2.2 mm). A comparison of the results for (a) 10 wt% and (c) 5 wt% indicated that the collision dynamics of droplets showed similar trends. However, small secondary droplets that were formed because of bursting vapor bubbles at the liquid–air interface were appreciably larger in number for a lower polymer concentration. The intensity of lightness in the dark areas for (c) 5 wt% appeared to be slightly higher than that for (a) 10 wt% because the amount of test polymer in the test solution was smaller for (c).

Figure 8 presents the time series of images showing the deformation behavior of aqueous polymer droplets impinging on the sapphire surface at T_w = 600 °C for (v, d) = (a) (1.5 m/s, 2.2 mm) and (b) (0.89 m/s, 2.2 mm). In the top view for (a), vapor bubbles formed inside the deforming droplets at 0.9 and 1.9 ms. At 2.8, 3.7, 4.3, and 5.4 ms, small secondary droplets were generated. The bursting of bubbles promoted the shuttering of the liquid. Unlike the previous results for T_w = 300–500 °C, no dark areas were observed in the interface view in any of the deformation stages.

3.2 Effect of varying Weber number on contact behavior of droplets with solid at high temperatures

This subsection describes the investigation of the effect of varying the Weber number associated with the impact inertia of solution droplets on the droplet dynamics in the substrate temperature range of 400–600 °C. A comparison of the side- and top-view images in Figures 6–8 for the 10 wt% solution droplets indicated that the spreading diameters of the droplet for We ≈ 30 were apparently smaller than those for We ≈ 100 because of the small impact inertia of the droplets. At 500 °C, the distorted droplet rebounded off the solid substrate for We ≈ 35, whereas the droplets split into pieces for We ≈ 100. At 600 °C, the shape of the droplet was roughly axisymmetric during the collision for We ≈ 35.

In our previous study [20], we reported that the critical Weber number, at which the

aqueous polymer solution droplet splits into pieces on a sapphire substrate, was approximately We = 60 when T_w = 500 °C. In the present experiments, we observed the disintegration of droplets when We = 53 and T_w = 500 °C, probably because of the higher liquid temperature and/or the mounting method of the solid substrate to the heater unit, which allowed slight movement of the substrate during droplet impact.

The contact behavior of the droplets for We ≈ 100 and We ≈ 30 showed similar trends. In both the cases, some dark areas were temporarily observed at T_w = 400 and 500 °C. The intensity of lightness in the dark areas for T_w = 500 °C was higher than that for T_w = 400 °C, and the lifetime of the dark areas was shorter. At 600 °C, no dark area was seen.

Next, the contact behavior of droplets was quantitatively compared by measuring the horizontal length of the liquid–solid contact area in the interface-view images. Figure 9 shows the time evolution of the liquid–solid contact diameter, which is defined in the figure, under the conditions of 500 °C for We = 101 and 32. A diameter of zero implies that no liquid–solid contact was observed. Because the liquid–solid contact area in the interface view was apparently asymmetric, particularly at later times as shown in Figure 7, the results for t < 7 ms are plotted in Figure 9. For We = 101, the contact diameters increased with time, reached a peak value (approximately 4.5 mm) at t ≈ 2 ms, and then remained constant. Thereafter, the diameter decreased (not shown in the figure). For We = 32, liquid–solid direct contact cannot be observed at very early times. The spreading rate of the contact diameter was smaller than that for We = 101 because of the smaller impact inertia of droplets. The maximum contact diameter was also slightly smaller. It was concluded that varying the Weber number had some effect on the formation process of the temporary polymer-enriched layer only at early times. Evidently, the temperature of the solid was a more important factor in the formation/disappearance of the dark areas.

3.3 Lifetime of polymer-enriched layer at high temperatures of solid

In this subsection, we describe the investigation of the critical temperature at which no temporary dark area formed on the solid substrate and the lifetime of the dark area (polymer-enriched layer) at a given temperature of the solid. The lifetimes of the polymer-enriched layer were determined based on naked-eye observations of numerous interface-view images taken at various flash timings. Figure 10 shows the relationship between the lifetime of the temporary polymer-enriched layer and the temperature of the solid. The lifetime of the temporary polymer-enriched layer was approximately 65 ms at 450 °C. The lifetime decreased as the temperature of the solid increased and reached zero at approximately 580 °C. The lifetime is independent of the Weber number.

The present study clearly found that the temporary polymer-enriched layer formed at substrate temperatures considerably higher than the temperature range for the thermal decomposition of the test polymer measured by the thermogravimetric curve (Figure 1). In actual spray cooling, coolant droplets impact a solid substrate frequently. Before the transient polymer-enriched layer formed by one droplet collision disappears, the impact of another droplet occurs. Hence, it is considered that the polymer-enriched layer can be stably formed at temperatures of the solid considerably higher than the temperature range for the thermal decomposition of the polymer. Because the thermal conductivity and thermal diffusivity of sapphire are comparable to those of steel alloys like stainless steel, the present results will be true for quench hardening of steel products using spray cooling.

In actual industrial cooling, steel surface is conditionally oxidized. The thermal conductivity of oxidized scale is much smaller than that of the base metal. To simulate this case, we attempted to perform similar experiments using a synthetic quartz glass prism, which has a considerably lower thermal conductivity than sapphire, and is comparable to oxidized scale of FeO [43]. At T_w = 500 °C, an apparently darker wet area than that in the case of sapphire was observed; however, these results are not presented in this paper. For the case of water- synthetic quartz glass, the interfacial temperature calculated by Eq. (2) using the thermo-physical properties listed in Table 3

was approximately 304 °C, which was close to the superheat limit of water. In addition, we could not determine the temperature of the synthetic quartz substrate to confirm the zero lifetime of the polymer-enriched layer, because of the restriction of heater power. Further, unlike in the case of the sapphire substrate, a very small amount of char always remained on the solid surface even when the temperatures of the solid substrate were higher than 400 °C. These results indicated that the lifetime curve shown in Figure 10 was valid only under the present experimental conditions and was influenced by other parameters such as the thermo-physical properties of the solid. Further analysis of this topic is a challenge that will be considered in future studies.

4. Conclusions

The deformation and contact behavior of polymer solution droplets impinging on hot substrates were investigated experimentally. The results are summarized as follows:

1. A three-directional flash photography method was developed. This observation technique can capture the time evolution of the droplet shape and the liquid–solid contact area simultaneously. The flow visualization technique was useful to understand the physics of phenomena in the collision of droplets with a solid.

2. The Weber number considerably influenced the deformation behavior of droplets. For We ≈ 100, the droplet impacted the solid substrate, spread, and split into pieces because of bursting boiling bubbles at the free surface and/or large impact inertia. For We ≈ 30 and high temperatures of the solid substrate, the droplet rebounded off the solid. On the other hand, the behavior of the polymer-enriched layer formed on the solid surface was almost independent of the Weber number except at early times. The temperature of the solid substrate was a dominant parameter governing the behavior of the polymer-enriched layer.

3. A polymer-enriched layer formed temporarily at substrate temperatures higher than the temperature range for thermal decomposition measured by the thermogravimetric

curve. The lifetime of this temporary polymer-enriched layer decreased as the substrate temperature increased. No polymer-enriched layer formed when a polymer solution droplet impacted a sapphire substrate heated above approximately 580 °C.

Funding

This work was supported by the Japan Society for the Promotion of Science through a Grant-in-Aid for Scientific Research (c) [grant number 15K05825].

Acknowledgement

The authors would like to thank Mr. Takahiko Okamoto of Daido Chemical Industry Co. Ltd. for his fruitful discussion and valuable support in preparing the test aqueous polymer solutions.

References

[1] G.E. Totten, C.E. Bates, N.A. Clinton, Handbook of Quenchants and Quenching Technology, ASM International, Materials Park, Ohio, 1993, ISBN 0-87170-448-X.

[2] A.K. Sinha, B.P. Division, ASM Handbook, Volume 4: Heat Treating, ASM International, Materials Park, Ohio, 1991, pp. 601–619, ISBN 0-87170-379-3.

[3] H.M. Tensi, A. Stich, G.E. Totten, Fundamentals About Quenching by Submerging, in: G.E. Totten, R.A. Wallis (Eds.), Proceedings of International Heat Treating Conference: Equipment and Process, 18–20 April 1994, Schaumburg, Illinois, ASM International, Materials Park, Ohio, 1994, pp. 243–251.

[4] G. Ramesh, K.N. Prabhu, Effect of polymer concentration on wetting and cooling performance during immersion quenching, Metall. Mater. Trans. B 47 (2) (2016) 859–881.

[5] D. Rodman, C. Krause, F. Nurnberger, F.W. Bach, K. Haskamp, M. Kastner, E. Reithmeier, Induction hardening of spur gearwheels made from 42CrMo4 hardening and tempering steel by employing spray cooling, Steel Res. Int. 82 (4) (2011) 329–336.

[6] D. Rodman, V. Boiarkin, F. Nurnberger, A. Dalinger, M. Schaper, Modeling of spray cooling during induction hardening of spur gearwheels made from 42CrMo4 hardening and tempering steel, Steel Res. Int. 85 (5) (2014) 741–755.

[7] G. Liang, I. Mudawar, Review of spray cooling – Part 1: Single-phase and nucleate boiling regimes, and critical heat flux, Int. J. Heat Mass Transf. 115 (2017) 1174–1205.

[8] G. Liang, I. Mudawar, Review of spray cooling – Part 2: High temperature boiling regimes and quenching applications, Int. J. Heat Mass Transf. 115 (2017) 1206–1222.

[9] M. Rein, Phenomena of liquid drop impact on solid and liquid surfaces, Fluid Dyn. Res. 12 (2) (1993) 61–93.

[10] M. Rein, Interactions between drops and hot surfaces, in: M. Rein (Ed.), Drop-Surface Interactions, Springer-Verlag Wien, New York, 2002, pp. 185–217.

[11] A.L. Yarin, Drop impact dynamics: Splashing, spreading, receding, bouncing…, Ann. Rev. Fluid Mech. 38 (2006) 159–192.

[12] S.T. Thoroddsen, T.G. Etoh, K. Takehara, High-speed imaging of drops and bubbles, Ann. Rev. Fluid Mech. 40 (2008) 257–285.

[13] D. Quere, Leidenfrost dynamics, Ann. Rev. Fluid Mech. 45 (2013) 197–215.

[14] G. Liang, I. Mudawar, Review of mass and momentum interactions during drop impact on a liquid film, Int. J. Heat Mass Transf. 101 (2016) 577–599.

[15] G. Liang, I. Mudawar, Review of drop impact on heated walls, Int. J. Heat Mass Transf. 106 (2017) 103–126.

[16] A. Rozhkov, B. Prunet-Foch, M. Vignes-Adler, Impact of drops of polymer solutions on small targets, Phys. Fluids 15 (7) (2003) 2006–2019.

[17] V. Bertola, Drop impact on a hot surface: Effect of a polymer additive, Exp. Fluids 37 (5) (2004) 653–664.

[18] V. Bertola, K. Sefiane, Controlling secondary atomization during drop impact on hot surfaces by polymer additives, Phys. Fluids 17 (10) (2005) 108104.

[19] D. Zang, X. Wang, X. Geng, Y. Zhang, Y. Chen, Impact dynamics of droplets with silica nanoparticles and polymer additives, Soft Matter 9 (2) (2013) 394–400.

[20] H. Fujimoto, S. Watanabe, T. Okamoto, T. Hama, H. Takuda, Photographic study of hydrodynamics of drops of aqueous polymer solution impinging on hot solid, Exp. Therm. Fluid Sci. 60 (2015) 66–74.

[21] H. Fujimoto, Y. Oku, T. Ogihara, H. Takuda, Hydrodynamics and boiling phenomena of water droplets impinging on hot solid, Int. J. Multiph. Flow 36 (8) (2010) 620–642.

[22] P. I. Freeman, J.S. Rowlinson, Lower critical points in polymer solutions, Polymer 1 (1960) 20–26.

[23] N. Nagai, S. Nishio, Leidenfrost temperature on an extremely smooth surface, Exp. Therm. Fluid Sci. 12 (3) (1996) 373–379.

[24] H. Fujimoto, H. Shiraishi, N. Hatta, Evolution of liquid/solid contact area of a drop impinging on a solid surface, Int. J. Heat Mass Transf. 43 (9) (2001) 1673–1677.

[25] V.P. Skripov, Metastable Liquids, John Wiley and Sons, New York, 1974, p. 83–177.

[26] C.T. Avedisian, The homogeneous nucleation limits of liquids, J. Phys. Chem. Ref. Data 14 (1985) 695–729.

[27] J.H. Lienhard, Correlation for the limiting liquid superheat, Chem. Eng. Sci. 31 (9) (1976) 847–849.

[28] M.N. Hasan, M. Monde, Y. Mitsutake, Lower limit of homogeneous nucleation boiling explosion for water, Int. J. Heat Mass Transf. 54 (15) (2011) 3226–3233.

[29] K.P. Derewnicki, Experimental studies of heat transfer and vapour formation in fast transient boiling, Int. J. Heat Mass Transf. 28 (11) (1985) 2085–2092.

[30] Y. Iida, K. Okuyama, K. Sakurai, Boiling nucleation on a very small film heater subjected to extremely rapid heating, Int. J. Heat Mass Transf. 37 (17) (1994) 2771–2780.

[31] C.T. Avedisian, W.S. Osborne, F.D. Mcleod, C.M. Curley, Measuring bubble nucleation temperature on the surface of a rapidly heated thermal ink-jet heater immersed in a pool of water, Proc. R. Soc. Lond. A: Math. Phys. Eng. Sci. 455 (1991) (1999) 3875–3899.

[32] S. Glod, D. Poulikakos, Z. Zhao, G. Yadigaroglu, An investigation of microscale explosive vaporization of water on an ultrathin Pt wire, Int. J. Heat Mass Transf. 45 (2) (2002) 367–379.

[33] O.C. Thomas, R.E. Cavicchi, M.J. Tarlov, Effect of surface wettability on fast transient microboiling behavior, Langmuir 19 (15) (2003) 6168–6177.

[34] Y. Hong, N. Ashgriz, J. Andrews, Experimental study of bubble dynamics on a micro heater induced by pulse heating, J. Heat Transf. 126 (2) (2004) 259–271.

[35] M. Seki, H. Kawamura, and K. Sanokawa, Transient temperature profile of a hot wall due to an impinging liquid jet, ASME J. Heat Transf. 100 (1978) 167–169.

[36] S.D. Aziz, S. Chandra, Impact, recoil and splashing of molten metal droplets, Int. J. Heat Mass Transf. 43 (2000) 2841–2857.

[37] J.D. Bernardin, I. Mudawar, The Leidenfrost point: Experimental study and assessment of existing models, ASME J. Heat Transf. 121 (1999) 894–903.

[38] J.D. Bernardin, I. Mudawar, A cavity activation and bubble growth model of the Leidenfrost point, ASME J. Heat Transf. 124 (2001) 864–874.

[39] J.D. Bernardin, I. Mudawar, A Leidenfrost point model for impinging droplets and sprays, ASME J. Heat Transf. 126 (2004) 272–278.

[40] G.E. Cossali, M. Marengo, M. Santini, Thermally induced secondary drop atomisation by single drop impact onto heated surfaces, Int. J. Heat Fluid Flow 29 (2008) 167–177.

[41] M. Furuya, T. Arai, Effect of surface property of molten metal pools on triggering of vapor explosions in water droplet impingement, Int. J. Heat Mass Transf. 51 (2008) 4439–4446.

[42] H.S. Carslaw, J.C. Jaeger, Conduction of Heat in Solids, second ed., Oxford University Press, Oxford, 1959, p. 88.

[43] M. Li, R. Endo, M. Akoshima, M. Susa, Temperature dependence of thermal diffusivity and conductivity of FeO scale produced on iron by thermal oxidation, ISIJ Int., 57 (2017), 2097–2106

List of figure and table captions

Table.1 Physical properties of water and test polymer solution

Type of liquid	Density (10^3 kg/m^3)	Surface tension (mN/m)	Viscosity (mm^2/s)	Specific heat (kJ/kgK)	Thermal conductivity (W/mK)
water (40 °C)	0.992	69.6	0.658	4.18	0.628
test liquid (10wt%)					
(20 °C)	1.09	53.6	10.0	4.00	0.543
(40 °C)	1.03	52.0	5.41	4.01	0.588
(50 °C)	0.997	51.3	4.18	4.02	0.593
(80 °C)	0.984	50.4	1.64	4.04	0.606

Table.2 List of experimental conditions

	Solid temperature (°C)	Liquid temperature (°C)	Droplet diameter (mm)	Impact velocity (m/s)	Weber number
Figure 3	300	30	2.4	1.6	84
Figure 5	300	30	2.2	1.6	106
Figure 6 (a)	400	30	2.2	1.5	103
Figure 6 (b)	400	40	2.2	0.9	32
Figure 6 (c)(Water)	400	30	2.4	1.7	106
Figure 7 (a)	500	30	2.2	1.5	101
Figure 7 (b)	500	50	2.2	0.9	32
Figure 7 (c)(5 wt%)	500	35	2.2	1.5	-
Figure 8 (a)	600	30	2.2	1.5	102
Figure 8 (b)	600	50	2.2	0.9	34

Table 3 Thermo-physical properties of water, sapphire, and synthetic quartz glass to estimate water–solid interfacial temperatures.

	Temperature (°C)	Density (10^3 kg/m)	Specific heat (kJ/kg/K)	Thermal conductivity (W/m/K)
Sapphire	400	3.93	1.14	16.3
Sapphire	500	3.92	1.19	13.6
Synthetic quartz	500	2.19	1.12	2.10
Water	30	0.997	4.18	0.614
Water	50	0.988	4.18	0.645

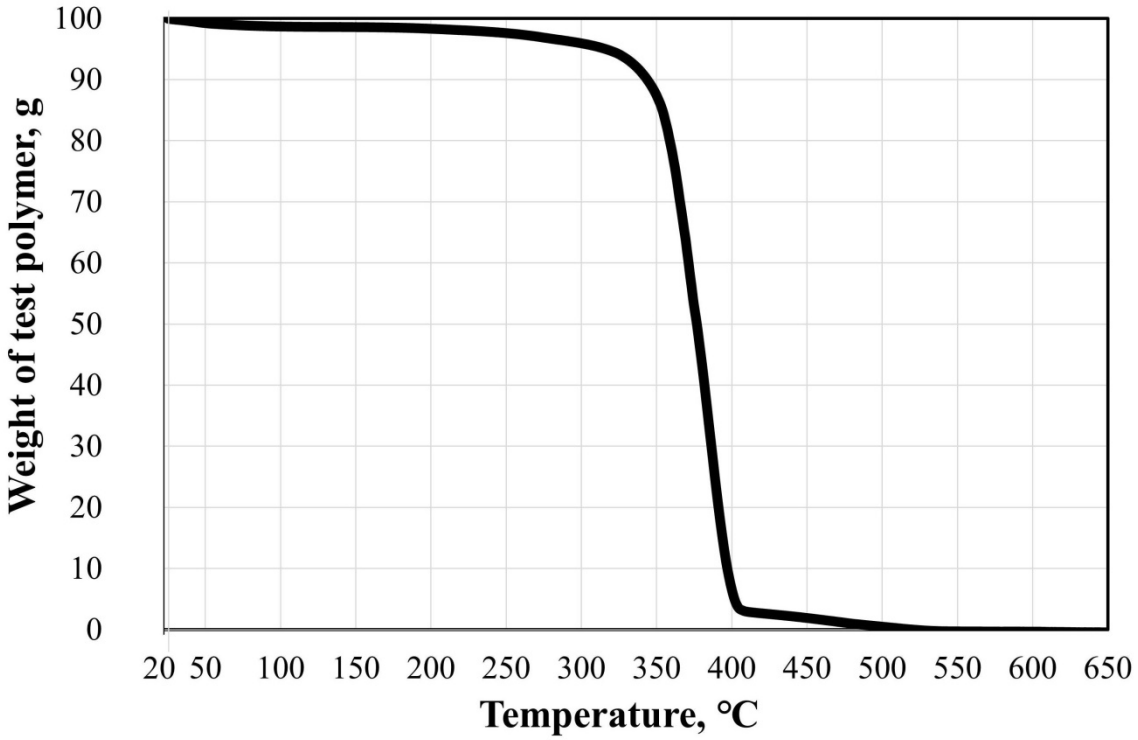

Fig.1 Thermo-gravimetric curve of test polymer

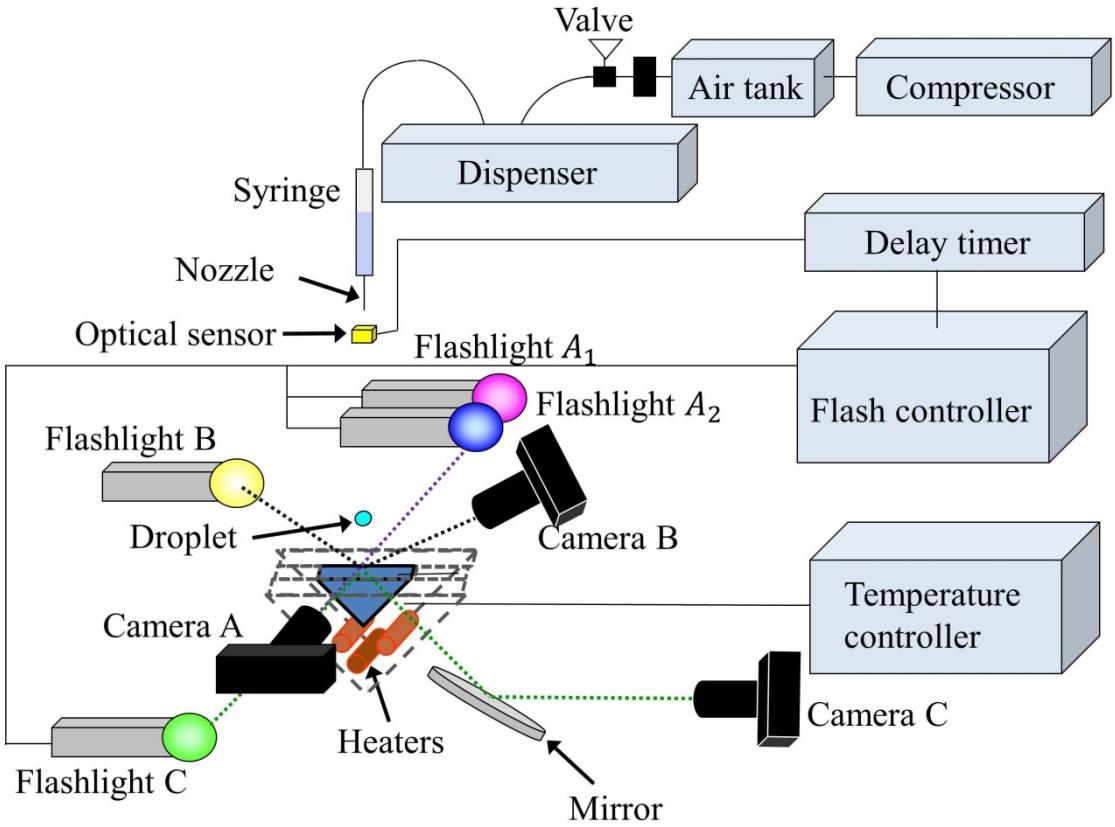

Fig.2 Schematic diagram of experimental setup

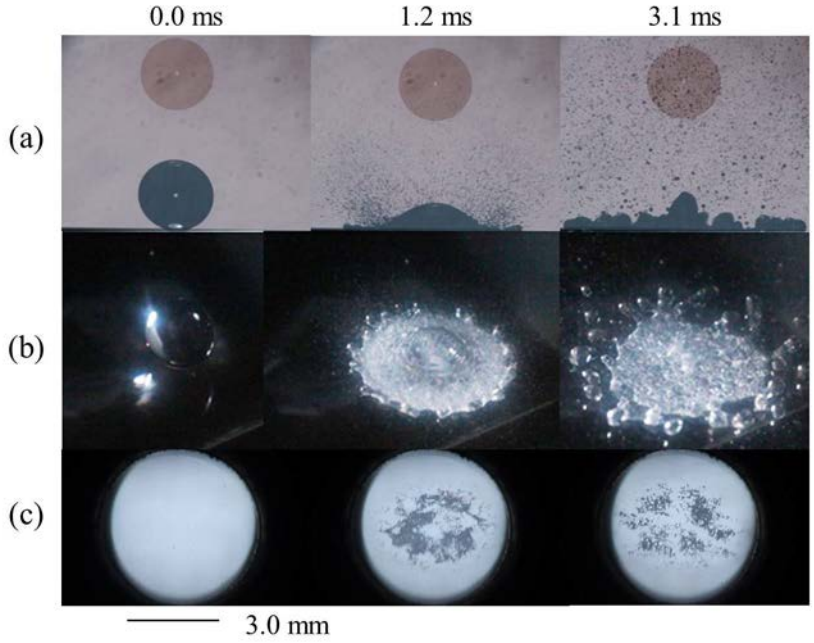

Fig.3 Examples of captured images using present photography system taken by (a) camera A, (b) camera B, and (c) camera C.

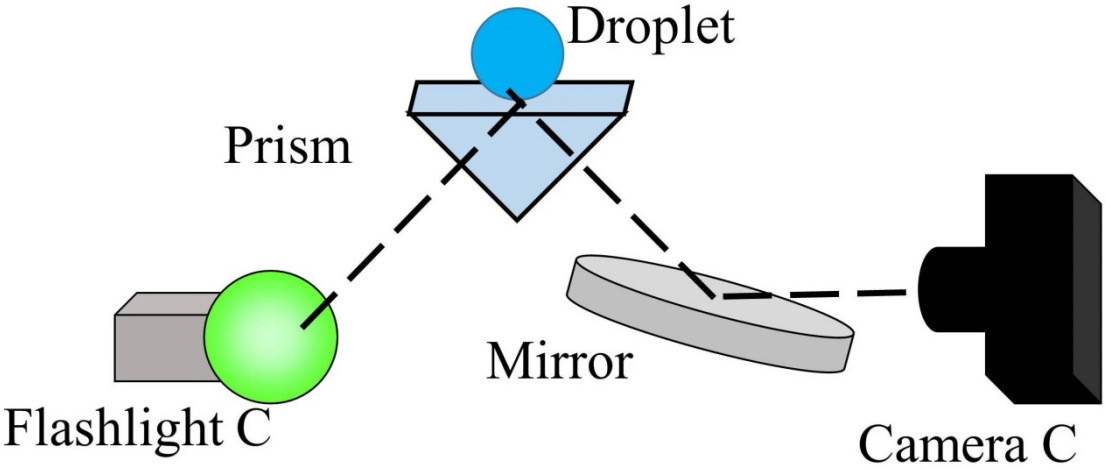

Fig.4 Schematic of photography for capturing liquid-solid interface

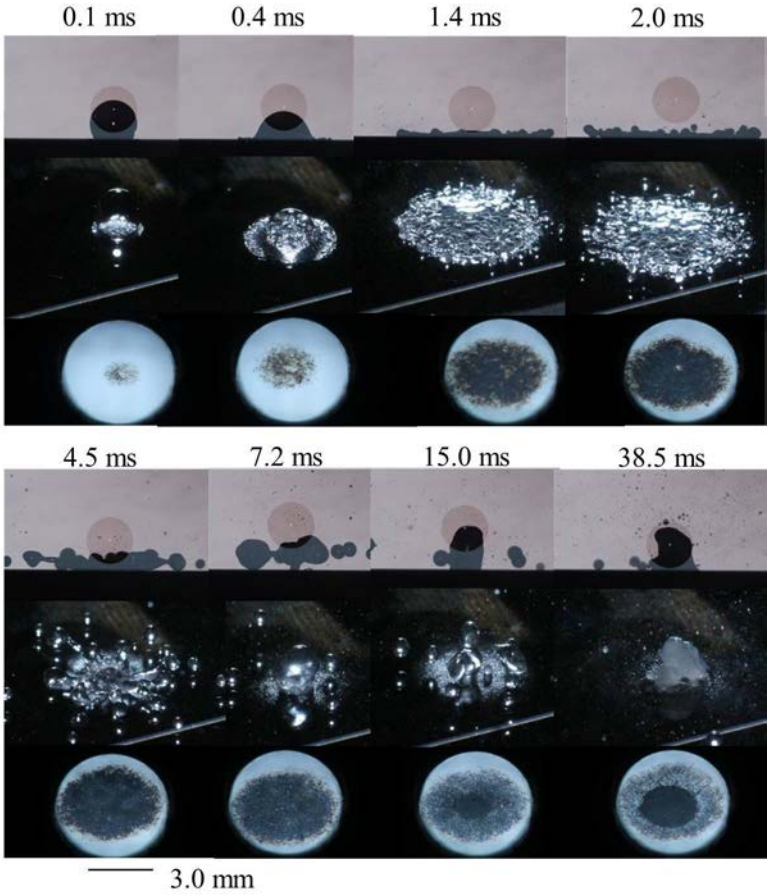

Fig.5 Deformation and contact behaviors of aqueous solution of polymer droplets impinging on sapphire surface at 300 ℃ for We=106

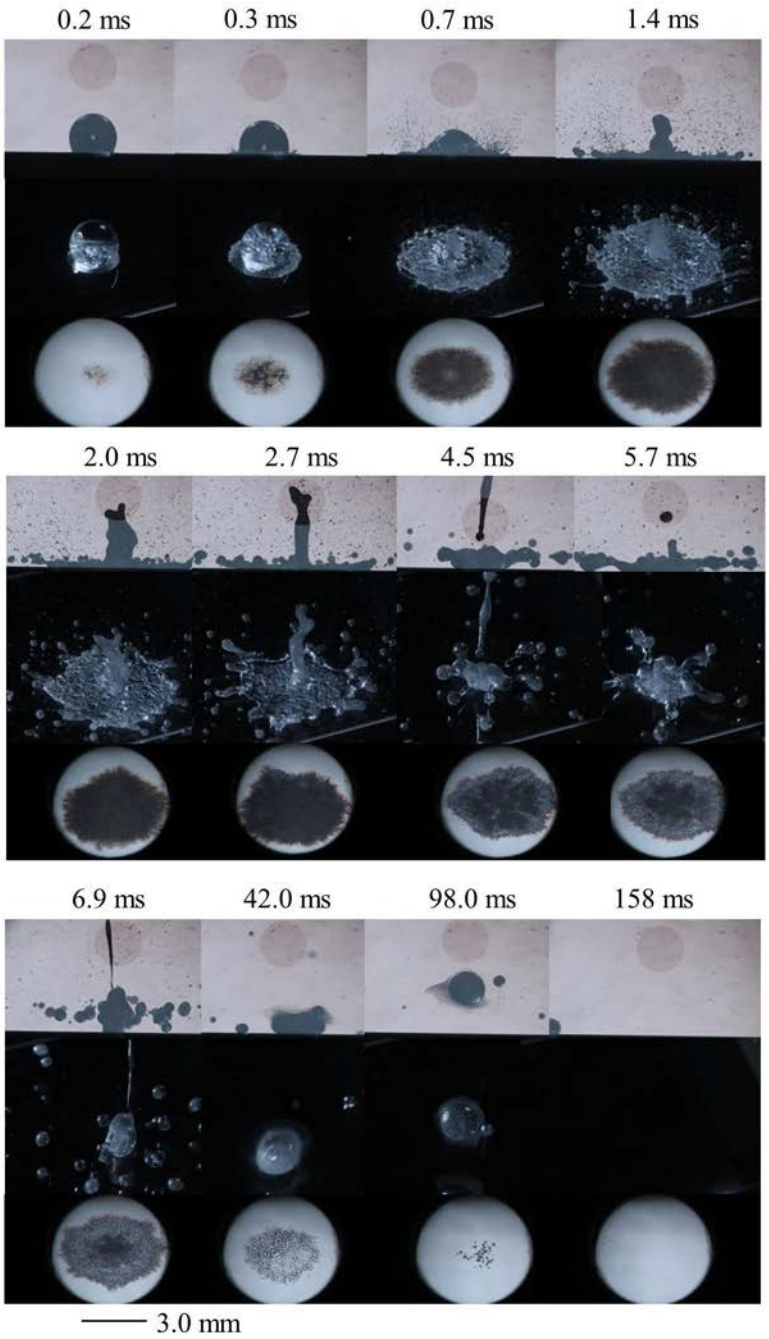

Fig.6(a)

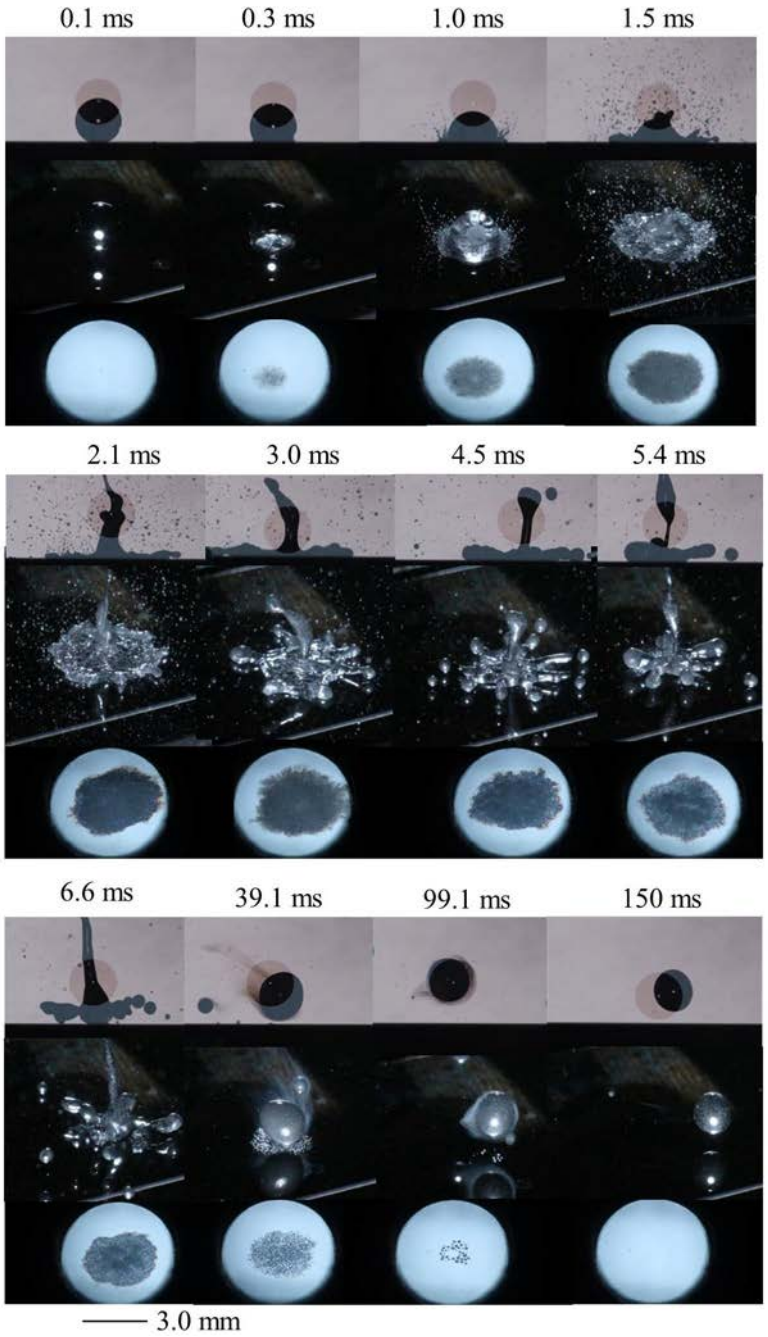

Fig.6(b)

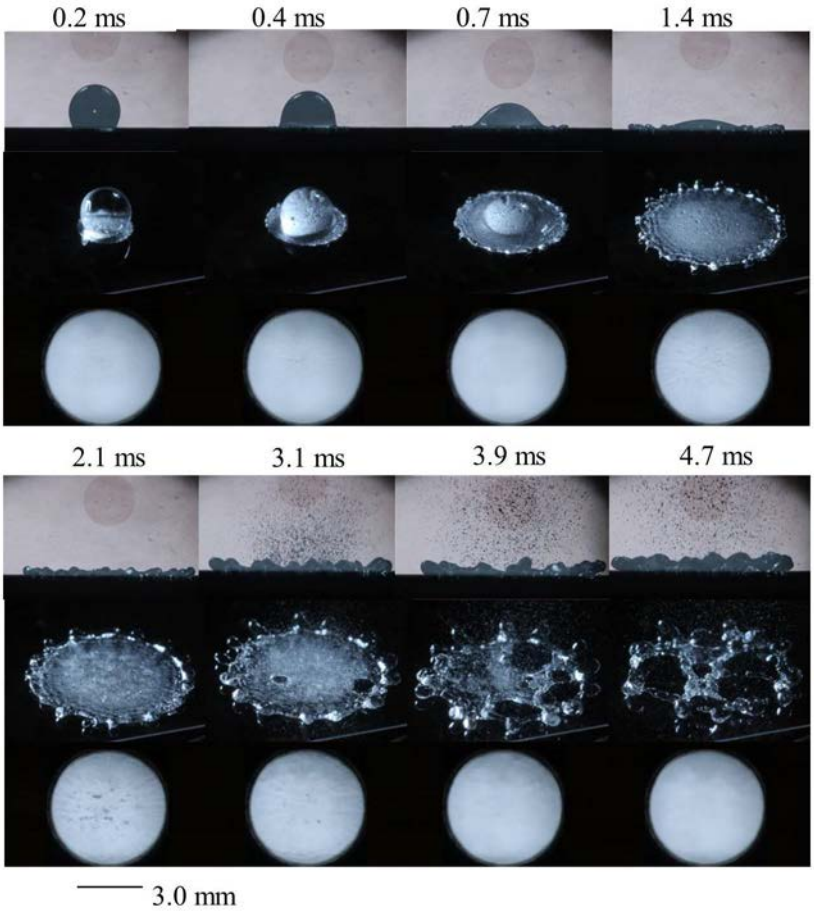

Fig.6(c)

Fig.6 Images of aqueous polymer solution droplets for (a) We=103 and (b) We=32 at 400 °C, and (c) images of water droplets for We=106

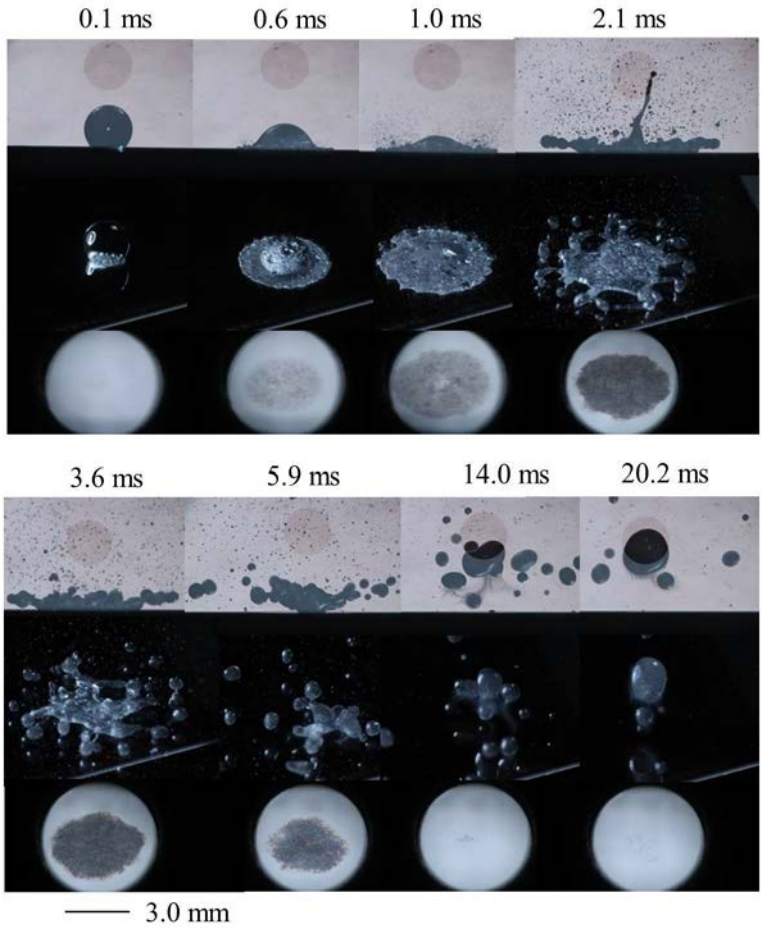

Fig.7(a)

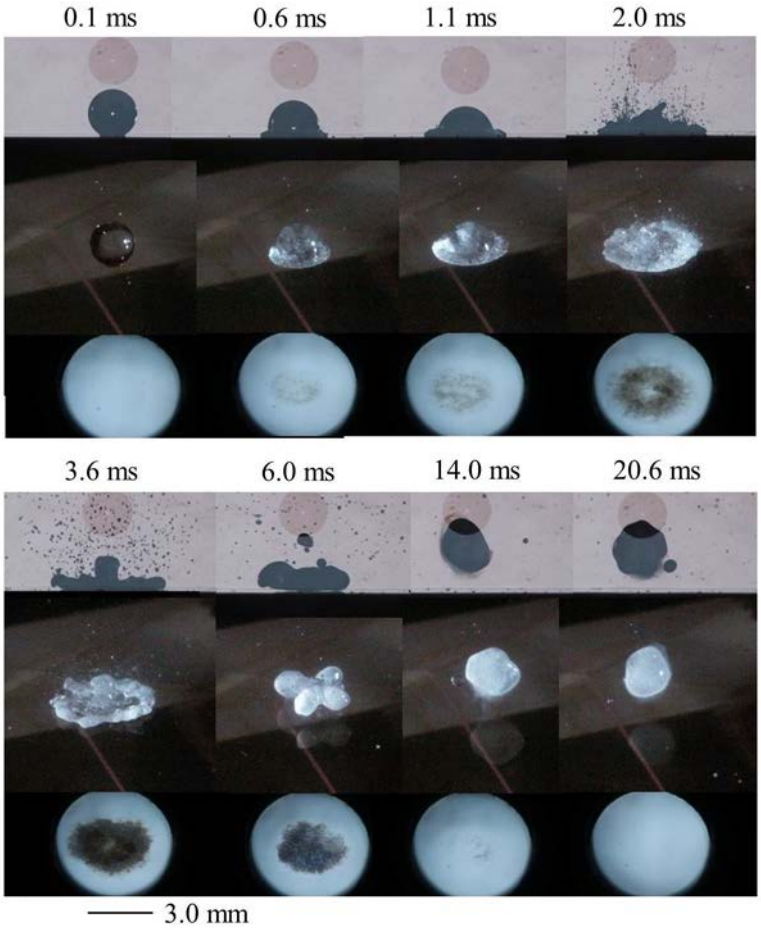

Fig.7(b)

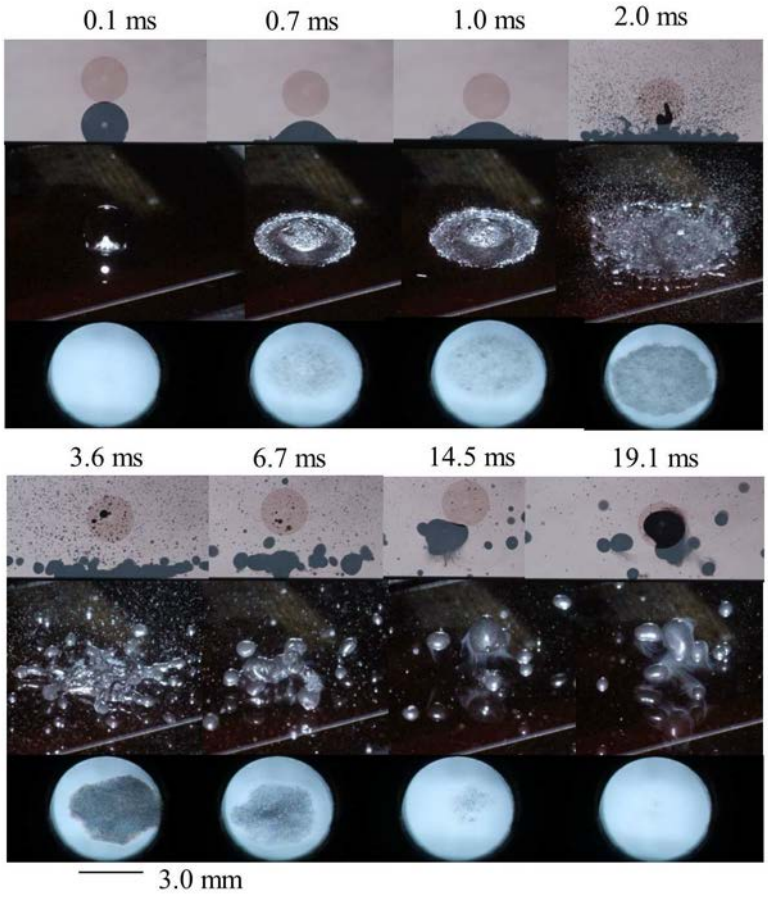

Fig.7(c)

Fig.7 Images of aqueous polymer solution droplets at 500 °C for (a) We=101 and (b) We=32, and (c) images of 5 wt% polymer solution droplets

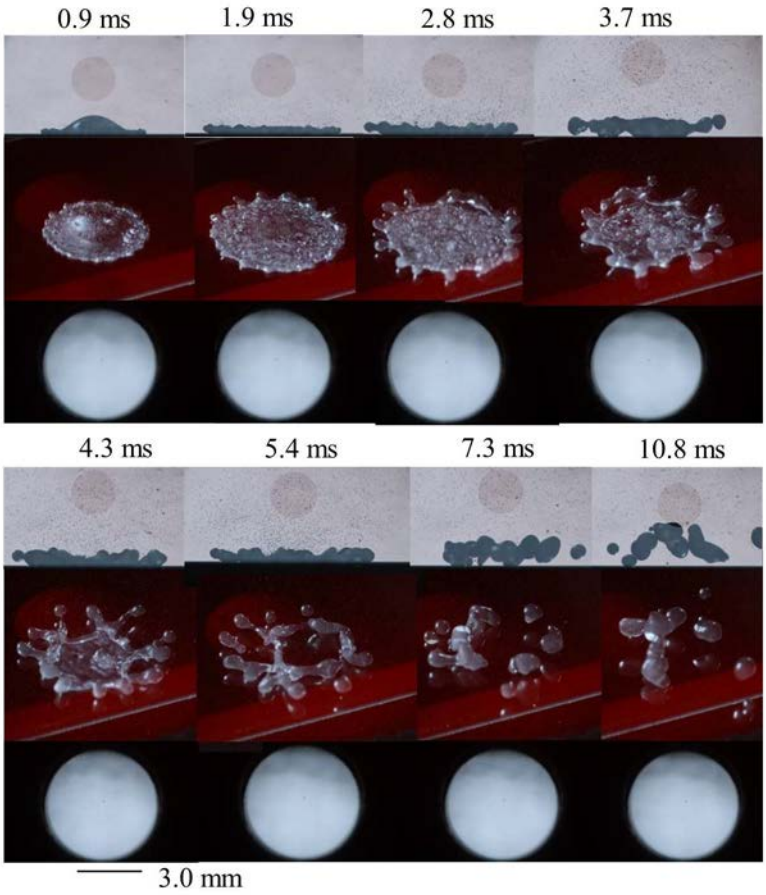

Fig.8(a)

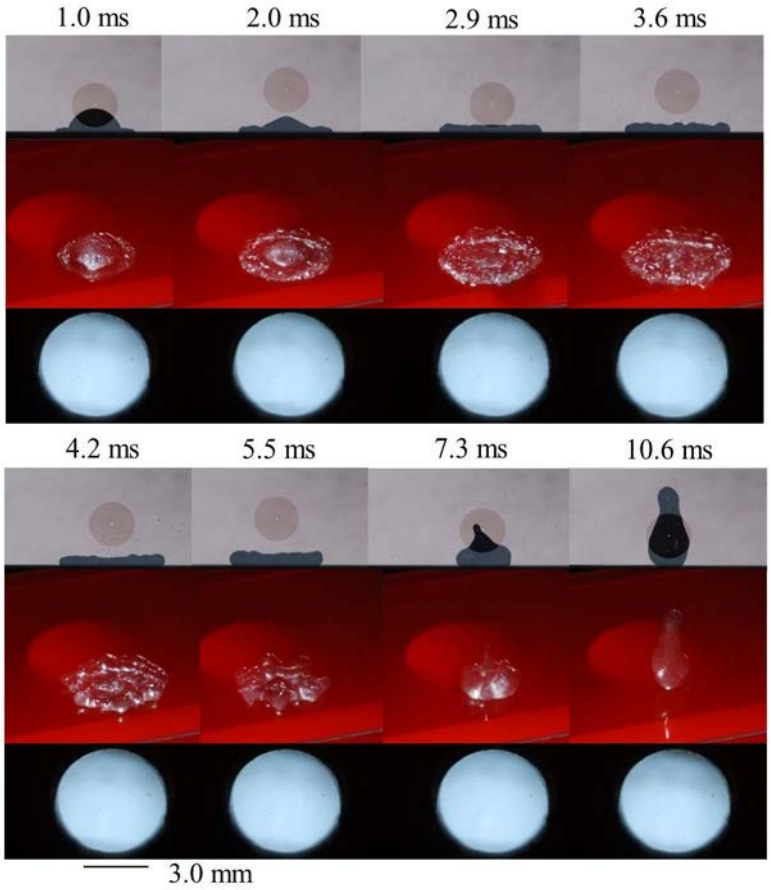

Fig.8(b)

Fig.8 Images of aqueous polymer solution droplets at 600 °C for (a) We=102 and (b) We=34

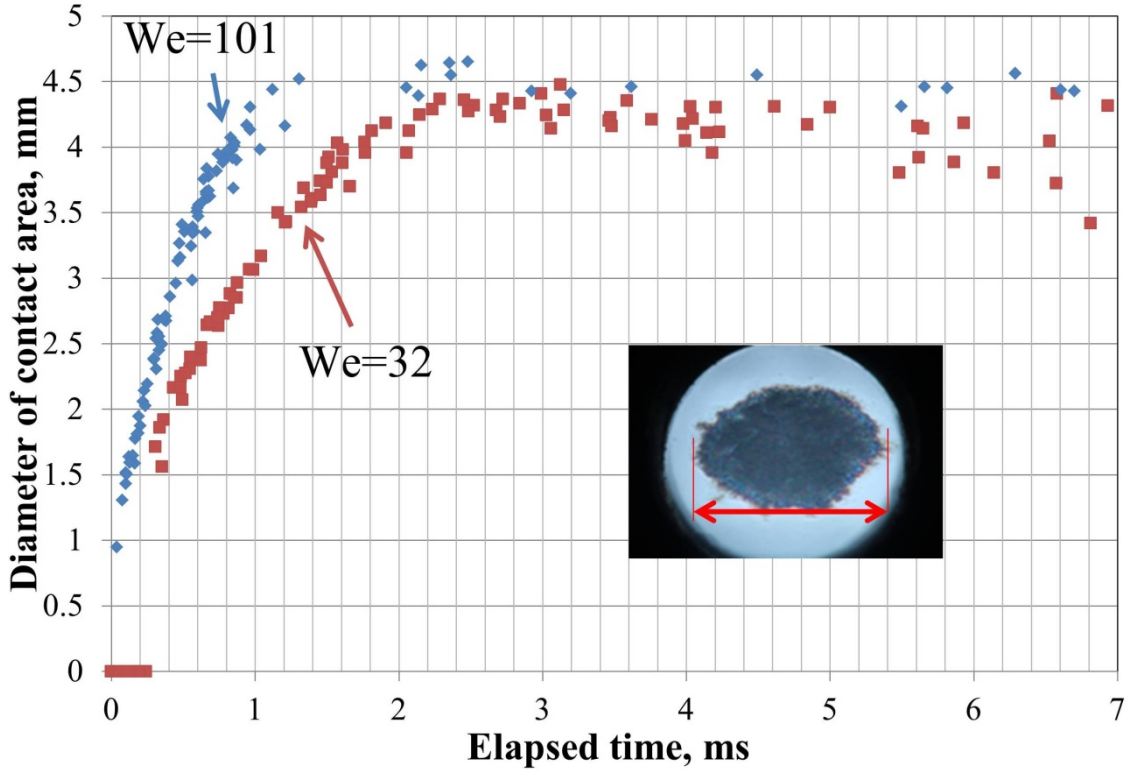

Fig.9 Time evolution of contact diameters for We=101 and 32 at 500 °C

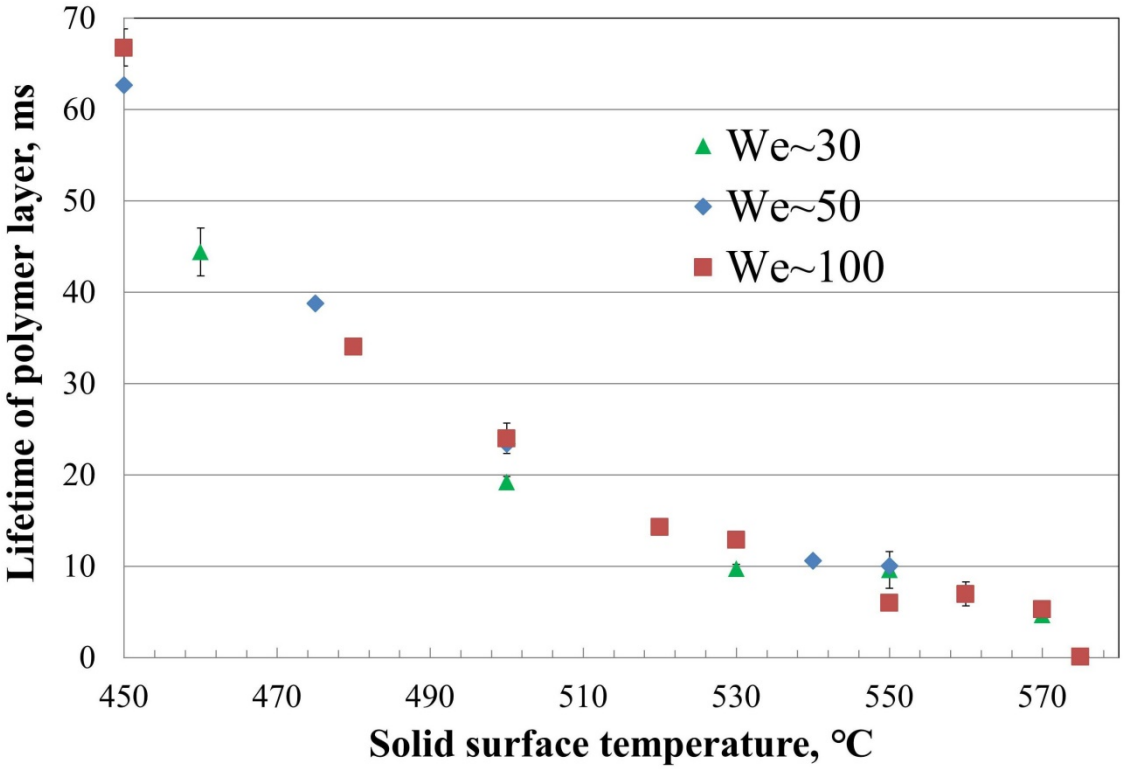

Fig.10 Lifetime of the temporary polymer-enriched layer